Desalination and Water Treatment
www.deswater.com

doi:10.5004/dwt.2017.20918

82 (2017) 241–251
July

Synthesis and characterization of magnetic nano-porous graphene functionalized with carboxyl for hexavalent chromium adsorption in aqueous solution

Sanaz Fathi[a], Roshanak Rezaei Kalantary[b,*], Alimorad Rashidi[c], Abdolreza Karbassi[d]

[a]*Department of Environmental Science, Faculty of Environment and Energy, Tehran Science and Research Branch, Islamic Azad University, Tehran, Iran, email: sanazfathi2@gmail.com*
[b]*Research Center for Environmental Health Technology (RCEHT), Iran University of Medical Sciences, Tehran, Iran, Tel. +98 21 86704775, Fax +98 21 86709487, email: rezaei.r@iums.ac.ir,*
[c]*Nanotechnology Research Center, Research Institute of Petroleum Industry (RIPI), Tehran, Iran, email: rashidiam@gmail.com*
[d]*Graduate Faculty of Environment, University of Tehran, P.O. Box 14155-6135, Tehran, Iran, email: akarbasi@ut.ac.ir*

Received 26 December 2016; Accepted 10 May 2017

ABSTRACT

In the present study, magnetic nano-porousgraphene (NPG) was synthesized and functionalized with carboxyl (COOH) in order to fabricate a recoverable magnetic composite (COOH@NPG/Fe_3O_4) as an adsorbent to remove hexavalent chromium (Cr(VI)) from aqueous solution. The synthesized adsorbent was also assimilated for higher efficiency and faster separation of pollutants from aqueous solutions. For magnetization of the adsorbent, nano-porousgraphene (NPG) was synthesized via chemical co-precipitation method and then functionalized with carboxyl (COOH). To minimize the adverse effects of magnetized nanoparticles, they can easily be separated by an external magnetic field. The morphological structure of adsorbent was characterized by several techniques (XRD, TEM, SEM, FTIR and VSM). The effect of various experimental parameters including solution pH, contact time, adsorbent dose, temperature and initial Cr(VI) concentrations was studied on the adsorption efficiency in batch experiments. The experimental equilibrium data had high correlation with the Langmuir isotherm and pseudo-second-order kinetic models, respectively. According to the obtained results of thermodynamic studies, the adsorption process was spontaneous and endothermic in nature and the adsorption process was optimum in higher temperature. The results suggested that COOH@NPG/Fe_3O_4 has a good potential for Cr(VI) removal in contaminated-wastewater treatment. The adsorbent can easily be separated from aqueous solutions and thus does not impose any secondary pollution in the environment.

Keywords: Water pollution; Heavy metal; Nano-adsorbent; Magnetic

1. Introduction

The accumulation of large concentrations of heavy metals in the biological systems, even at low levels, can lead to the imposing adverse effects to human life beings [1]. Among them, hexavalent chromium (Cr(VI)) is known as one of the most highly toxic heavy metals in wastewater that is abundant in different industrial effluents such as mining, battery, tanning and manufacturing. It also acts as a carcinogen, mutagen and teratogen agent in living organisms [2]. Research has shown that chromium ions can be found in both main oxidation states Cr(VI) and Cr(III) in aqueous solution. However, Cr(VI) is 500 times more toxic than Cr(III). Therefore, its removal from drinking water resources, especially at high concentrations, is of great importance[3,4]. When Cr(VI) is accumulated in human body, it could lead to adverse health effects and ultimately can be lethal at 0.1 mg/g body weight [5]. Until now, lots of various remediation methods like sedimentation [6] reduc-

*Corresponding author.

tion [7] ultra-filtration [8] and adsorption [9] have been applied to heavy metals removal from aqueous solutions. However, the aforementioned approaches may either generate a significant quantity of secondary waste products or achieve the discharge standards alone. The removal of Cr(VI) via precipitation technique has some disadvantages such as higher waste treatment equipment costs, large consumption of reagents and generation of high volumes of sludge. Although reverse osmosis and electro dialysis have high capability of removing Cr(VI), the reduction of high Cr(VI) concentration in the wastewaters to the permissible limit is quite difficult. In addition, ion exchange is an attractive approach in treating the wastewater containing Cr(VI), but the regeneration of resin and recovering pure chromic acid is practically difficult [10]. Adsorption is a conventional but efficient and environmental-friendly technique that now considered as a superior method for its cost-effectiveness and flexibility features. There are various adsorbents such as carbon materials (i.e. activated carbon, carbon nanotube and graphene) [11], purolite [12], activated alumina [13], biological waste [14], and coated silica gel [15] have been used for Cr-contaminated water treatment. In recent years, graphene has received great attention indifferent fields of research, due, in essence, to its wonderful physical and electrical properties like very large surface area, open porous structure, flexibility, chemical stability and high capacity for the sorption of pollutions from aqueous solution in a short-time [13–15]. These mentioned characteristics warrant it as a good candidate for constructing graphene-based composite materials. In this study, we used chemical vapor deposition (CVD) technique to synthesize nano-porous graphene (NPG) on transition metals that has recently been used for synthesizing large graphene domains [16,17]. The easily separation of adsorbents from aqueous media in order to not leading to secondary pollution in the soil and water resources is a high critical issue in environmental perspectives. Therefore, magnetic nanoparticles (MNPs) were prepared for synthesis of NPG/Fe_3O_4 as an adsorbent for the economic and efficient removal of Cr(VI) from aqueous solutions instead of using centrifugation and filtration that are time-consuming [18,19]. The adsorbent together with the adsorbed contaminants could be easily separated from solution by external magnetic field, due to its magnetism contributed from Fe_3O_4 [20]. Modification of graphene with different materials can produce various adsorbents for improving their adsorption capacity. Previous research have revealed that carboxyl groups derived sorbent had selective potential and good performance in several adsorbents such as carbon nanotubes and its application for contaminants removal [21,22].

The purpose of this work was to synthesize nano-porous graphene (NPG) by CVD method and magnetize it with MNPs (NPG/Fe_3O_4) for economic separation from water which was followed by functionalization with the carboxyl group to provide different nano-composite (COOH@NPG/Fe_3O_4) as an adsorbent for the removal of (Cr(VI)) ions from aqueous solutions. The characterization of COOH@NPG/Fe_3O_4 surface was carried out by several techniques such as vibrating sample magnetometer (VSM), transform infrared spectroscopy (FTIR), X-ray diffractometer (XRD), Scanning electron microscope (SEM) and Transmission on electron microscopy (TEM). The impacts of optimal parameters such as solution pH, contact time, temperature, initial ion concentrations and adsorbent dosage were studied. In addition, the adsorption experiments were conducted under varying conditions to investigate the equilibrium isotherms, kinetic models and thermodynamics.

2. Materials and methods

2.1. Materials

Anhydrous iron (III/II) chloride, (99.9%) ammonia solution, potassium dichromate and (28%) hydrazine hydrate were purchased from Merck, Co, Germany. A hand magnet (dimension of 5 × 4 × 4 cm and intensity of 1.3 T) was also applied for separation of adsorbent particles from solution. All the solutions were prepared by ultrapure water and kept at 4°C prior to use.

2.2. Preparation of nano-porous graphene (NPG)

Nano-porous graphene was fabricated using chemical vapor deposition (CVD) technique which is a highly effective and low-cost method as reported in the literature with a slight modification [23]. For synthesizing the porous adsorbent, graphene is formed on the metals such as copper [24]. This process is carried out in an electrical furnace consisting of a quartz tube with a diameter of 50 mm and 120 mm length. The furnace provided programmable heating up to 900–1100°C for 5–30 min [25]. The reaction was carried out using naphthalene as a source of carbon and by passing hydrogen gas in a ratio of 4:1. Nano-porous graphene was formed on the copper surface [23]. For both obtaining pure nano-porous graphene and metal nano-catalysts removal, the product was stirred in 18 % HCl solution for about 16 h at an ambient temperature (25 ± 2°C). Then, the sample was washed several times with distilled water. The washing process continued until the neutral material was obtained. Finally, the treated product was dried at 100°C [26].

2.3. Synthesis of magnetite nano-porous graphene (NPG/Fe_3O_4)

NPG/Fe_3O_4 nano-composite was fabricated via the reported method in the literature with insignificant changes. At the first stage, around 0.9 g of graphene was added into 250 ml of distilled water using ultra-sonication for 2 h at 60°C. Afterwards, mixture of 10 g $FeCl_3$ and 4 g $FeCl_2$ were poured into 25 ml of distilled water and then expose to N_2 gas for around 5–10 min. In the next step, 50% (w/v) NaOH was added to the mixture dropping singly to adjust the pH of solution at pH > 12. The solution temperature increased to 80°C. The as-synthesized solid particles were separated from solution via an external magnet, rinsed sequentially by means of ultrapure water and ethanol to remove any impurities. It was dried in a vacuum oven at 50°C for 24 h [27].

2.4. Functionalization of magnetite nano-porous graphene with carboxyl (COOH@NPG/Fe_3O_4)

Nano-porous graphene was functionalized by carboxyl. About 1 g of graphene was treated in 25 ml of nitric acid and 75 ml of sulfuric acid for 3 h at 60°C. The mixture was kept

in an ultrasonic bath and then washed by distilled water until reaching to the natural pH. Afterwards, the adsorbent was dried at 60°C for 8 h in an oven [28].

2.5. Characterization of the synthesis adsorbents

A scanning electron microscope (SEM, model MIRA3, Tescan, Czech Republic) was used to measure size, morphology and surface characteristics of the synthesized adsorbents. The XRD pattern of the adsorbent was prepared (Quantachrome, NOVA 2000) using graphite monochromatic copper radiation (Cu Ka, λ = 1.54 Å) in the 2θ range of 10–70° at 25°C. The morphological and shape of the adsorbent were recorded by a transmission electron microscope (TEM, model PHILIPS, EM 208 S) with 100 keV. In addition, the surface functional groups were characterized by fourier transform infrared spectroscopy (FTIR) (Tensor 27, Bruker, Germany). VSM (7400, Lakeshare) was also applied to determine the magnetic properties of adsorbent at 10 kOe at 25°C.

2.6. Batch adsorption experiment

The Cr(VI) stock solution (1000 mg/L) was prepared by dissolving certain amounts of $K_2Cr_2O_7$ in 1000 mL of deionized water. The solution pH was adjusted by 0.1 M NaOH and 0.1 M HCl solutions. The effect of operating parameters such as solution pH (2–10), contact time (5–120 min), adsorbent dose (20, 35, 50, 100, 150 and 200 mg/L), temperature (283, 298, 303 and 323K) and different initial Cr(VI) concentrations (25, 50, 100,150 and 200 mg/L) on the adsorption efficiency was investigated. To ensure the perfect mixing of the adsorbent with Cr(VI) in solution, the samples were agitated at 200 rpm for about 120 min. Subsequently, the adsorbents were magnetically separated from the solution using a hand magnet. The residual concentration of Cr(VI) in the solution was determined through colorimetric method via a spectrophotometer (7400CE CECIL) at 540 nm using diphenyl carbazine method. Finally, the adsorption capacity (q_e) and the removal efficiency (Re%) of Cr(VI) were determined through the following equations:

$$q_e(mg/g) = \left[\frac{C_0 - C_e}{W}\right] \quad (1)$$

$$\text{Re}\ (\%) = \left[\frac{C_0 - C_e}{C_0}\right] \times 100 \quad (2)$$

where C_0 and C_e (mg/L) are respectively the initial and residual Cr(VI) concentrations, and W (g/L) stands for the adsorbent mass to the volume of the solution.

2.7. Isotherm, kinetic and thermodynamic of adsorption

The Langmuir and Freundlich isotherm models were used to evaluate Cr(VI) adsorption onto the adsorbent are summarized in Table 1. For Langmuir isotherm model, the K_F (L/mg) is the empirical constant related to energy and q_m (mg/g) represents the maximum adsorption capacity. In the case of Freundlich isotherm model, the K_F and n are the Freundlich constants related to the adsorption capacity and intensity, respectively. The q_m and K_F parameters are calculated from the slope and intercept of the C_e/q_e plot vs. C_e, respectively. The Freundlich isotherm parameters (K_F and n) are also calculated from the slope and intercept of the ln C_e plot versus ln q_e, respectively.

In order to express the reaction between adsorbate and adsorbent, the experimental data were fitted with two kinetic models. Herein, two kinetic models including the pseudo-first-order and pseudo-second-order models were applied for the modeling of the adsorption of Cr(VI) onto COOH@NPG/Fe_3O_4. The linear equations of the mentioned models along with the respective parameters are given in Table 1, where q_t (mg/g) is the amount of adsorption capacity at a given time t; and, k_1, and k_2 are the rate constant of pseudo-first-order and pseudo-second-order sorption, respectively.

Thermodynamics of adsorption deals with the transformation of substance and energy in systems as they advance to acquire a balanced condition. In thermodynamic studies, the principles of normal enthalpy ($\Delta H°$), standard free energy ($\Delta G°$) and standard entropy ($\Delta S°$) are necessary. The values of $\Delta H°$, $\Delta S°$ and $\Delta G°$ are obtained by using the following equations:

$$\Delta G^\circ = -RT \ln K^\circ \quad (3)$$

$$\ln K^\circ = \Delta S^\circ / R - \Delta H^\circ / (RT) \quad (4)$$

where R is the universal gas constant (8.314 J/mol·K), T is the temperature (K). The sorption equilibrium constant ($K°$) can be calculated by plotting ln K_d versus C_e and extrapolating C_e to zero. $\Delta H°$ and $\Delta S°$ were obtained from the slope and intercept of Van't Hoff plots of ln (K^0) versus $1/T$, respectively [29].

Table 1
The linear equations and parameters of isotherm and kinetics of (Cr(VI)) ions adsorption onto COOH@NPG/Fe_3O_4

Models	Linear equations	Parameters	Plot
Kinetic			
Pseudo-first-order	$q_t = q_e[1 - \exp(k_1 \cdot t)]$	$q_{e,exp}$, k_f	$\ln(q_e - q_t)$ vs. t
Pseudo-second-order	$q_t = q_e - (q_e/[k_2(q_e) \cdot t + 1])$	$q_{e,exp}$, k_s	t/q_t vs. t
Isotherm			
Freundlich	$q_e = k_F(C_e)^{1/n}$	k_F, n	ln q_e vs. ln C_e
Langmuir	$q_e = (q_m k_L C_e)/(1 + k_L C_e)$	k_L, q_0	q_e vs. ln C_e

3. Results and discussion

3.1. Characterization of the synthesized adsorbent

Fig 1a shows the XRD diagram of porous graphene, Fe_3O_4 nanoparticles and nano-porous magnetic graphene. Based on the figure, Observation shows these peaks much less intensively in graphene and Fe_3O_4 NPs which reveals the presence of Fe_3O_4 particles in NPG/Fe_3O_4 structure that is a reliable proof for successful synthesis of nano-adsorbent with MNPs. The angle of the adsorbent was obtained in the range of 2θ = 5–80°, with the use of radiation Cu kα (λ = 1.5°A). The intense diffraction peaks at the bragg angles of 30.09, 35.42, 37.05, 43.05, 53.39, 56.94 and 62.51 correspond to the (2 2 0), (3 1 1), (2 2 2), (4 0 0), (4 2 2), (5 1 1) and (4 4 0) facets of the cubic spinal crystal planes of Fe_3O_4 (JCPDS card No. 19-0629), respectively. The carbon peak is marked at 2θ of 25°. Peaks related to the magnetite nano-particles (Fe_3O_4) on the absorbent structure are shown in the range of 45.5–55.6° [30].

According to Fig. 1b determining the magnetic characterize of COOH@NPG/Fe_3O_4 the VSM magnetization curve

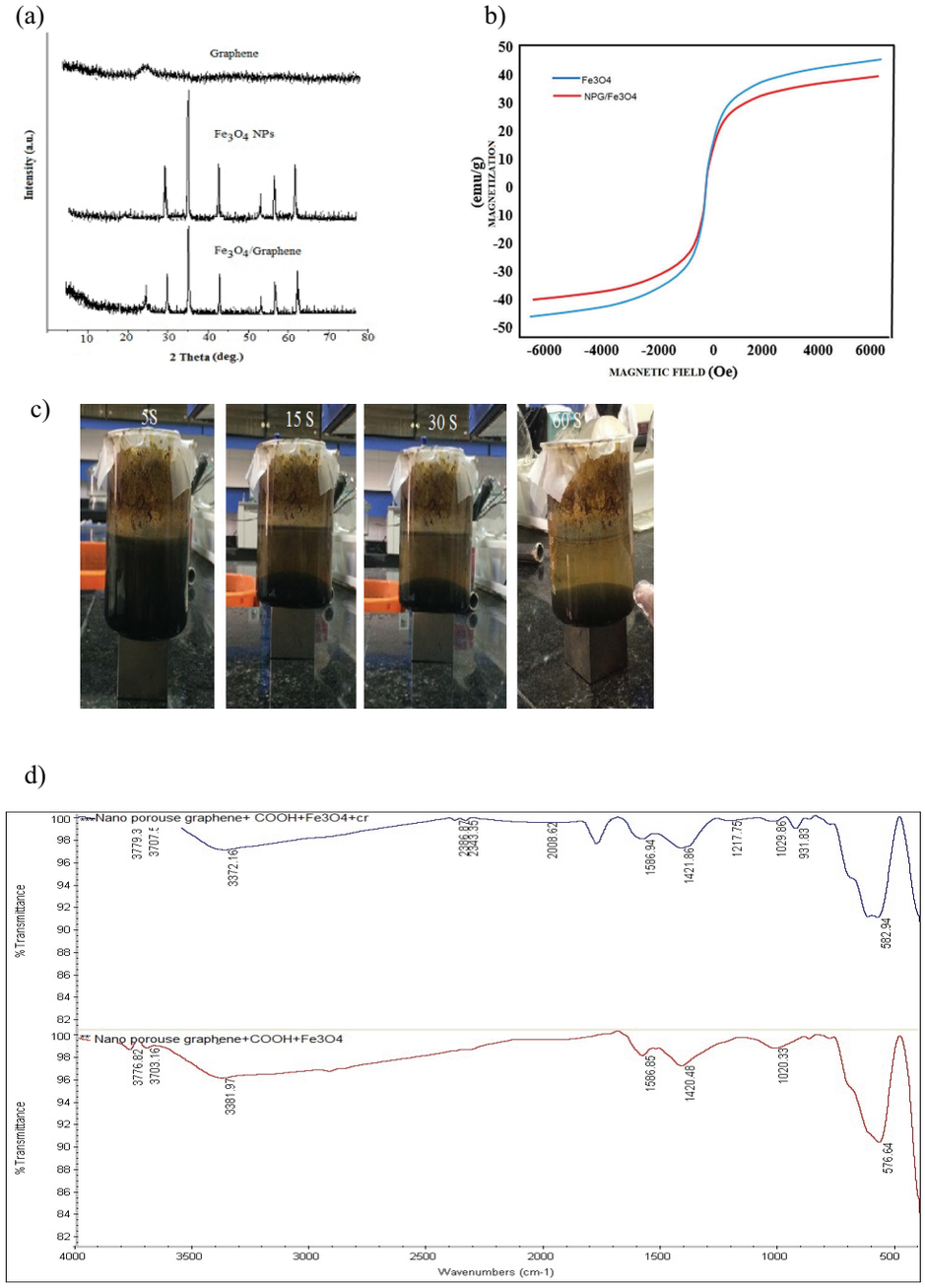

Fig. 1. XRD analysis of graphene, Fe_3O_4 NPs, and NPG/Fe_3O_4 (a), magnetization curve (b), photographs of the separation processes of adsorbent from solution with external magnetic field (c), FT-IR spectra of synthesis adsorbent (d),

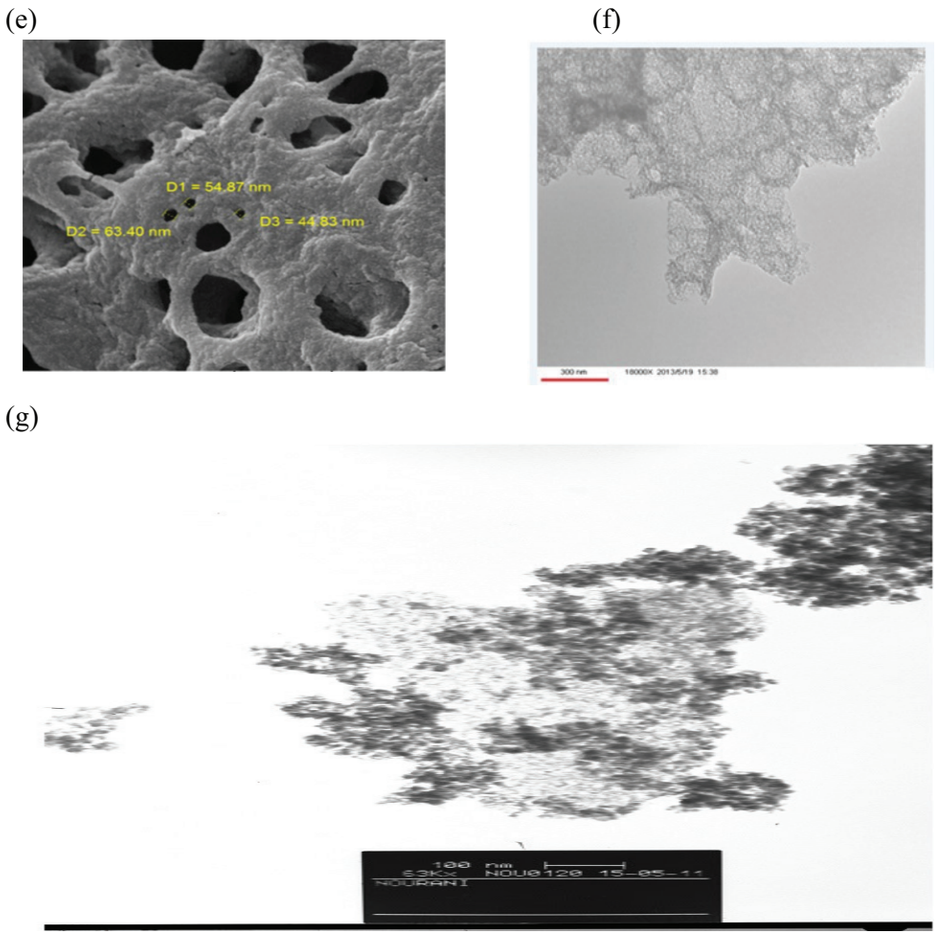

Fig. 1. XRD analysis of graphene, Fe_3O_4 NPs, and NPG/Fe_3O_4, TEM image of synthesized adsorbent in low-magnification (e), TEM image in high-magnification (f), and SEM image of adsorbent (g).

was achieved in magnetic field of ±10 kOe at 25°C. The highest magnetization saturation of 46.3 emu/g was obtained for Fe_3O_4, which was higher than that of COOH@NPG/Fe_3O_4. Maximum saturation of magnetization was about 35.2 emu/g, indicating that COOH@NPG/Fe_3O_4 can be easily separated from solutions and potentially employed as a recoverable magnetic adsorbent to remove pollutants from aqueous environment for hindering the secondary pollution. Fig. 1c shows an excellent magnetic response to a magnetic field and could be separated simply from solution with external magnetic field after 60 s.

Fig. 1d illustrates the FTIR spectra of synthesized composite of COOH@NPG/Fe_3O_4+(Cr(VI)) ions and COOH@NPG/Fe_3O_4which shows the functional groups onto the surfaces of adsorbent that is a very critical parameter in the adsorption process. View of magnetic nanoparticles at a wavelength of 582 cm^{-1} confirms the Fe–O bonds between groups are in the form of tetrahedron. The other groups that have emerged in the wavelength of 1421.86 cm^{-1} and 3312 cm^{-1} can be assigned to represents aromatic C=C bonds and OH stretching vibrations of the carboxylic acid group, respectively. Finally, alkoxy CO bond is defined at 1029 cm^{-1} which indicates the graphene structure of NPG. The peak around 1700 cm^{-1} appears in the spectra of COOH@NPG/Fe_3O_4+(Cr(VI)) ions [31,32]. In addition, Fig. 1e represents the morphology, size and surface area of the NPG analyzing by TEM in low-magnification which reveal good porosity and high adsorption capacity. With application of TEM technique, it could be pointed out that a high density of Fe_3O_4 nanoparticles is noticed on the NPG layers (Fig. 1f) high-magnification and Fig. 1g shows SEM image of adsorbent after functionalization.

3.2. *Effect of pH of solution on Cr(VI) adsorption onto COOH@NPG/Fe_3O_4*

The solution pH has always been considered as one of the most critical experimental variables that plays an important role in controlling the adsorption process. The Cr(VI) removal rate in various ranges of pH is shown in Fig 2. pH values changed from 2 to 8, while the other parameters including contact time, adsorbent dosage, initial Cr(VI) concentration, and agitation speed were kept constant at 2 h, 35 mg/L, 100 mg/L, and 200 rpm, respectively. The maximum Cr(VI) adsorption rate was found at

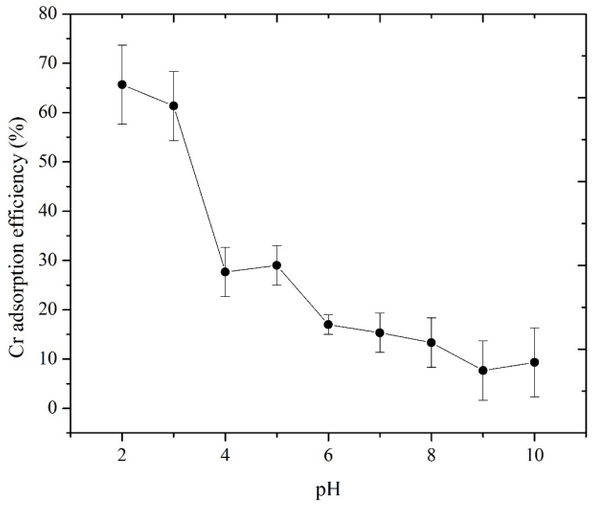

Fig. 2. Effect of pH on the adsorption of Cr(VI) onto COOH@NPG/Fe_3O_4 (Time: 90 min, adsorbent dosage = 35 mg/L, initial Cr (VI) concentration = 100 mg/L and agitation speed = 200 rpm).

pH range 2–3. The high Cr(VI) removal rate at acidic pH conditions would be attributed to the neutralization of surface negative charges of the adsorbents in the presence of excessive amount of hydrogen ions. According to a similar study, the adsorption of (Cr(VI)) ions on COOH@NPG/Fe_3O_4 was significant at acidic conditions [33–35]. Cr(VI) may exist in different ionic states, which in turn facilitates the diffusion of the hydrogen chromate ion ($HCrO_4^-$) and its subsequent adsorption. Dichromate ions ($Cr_2O_7^{2-}$) under acidic conditions reduces to Cr(III) as express below:

$$Cr_2O_7^{2-} + 14H^+ + 6e^- \rightarrow 2Cr_3^{2+} + 7H_2O \;\; E^\circ = 1.33V \quad (5)$$

However, in basic solutions it is much less oxidizing and exists as $Cr(OH)_3$ [36,37]:

$$Cr_2O_7^{2+} + 4H_2O + 3e^- \rightarrow Cr(OH)_3 + 5OH^- \quad E^\circ = -0.13V \quad (6)$$

The most probable reason of this phenomenon would be the positive surface charges of adsorbent at low pH values. In other words, the high removal efficiency of Cr(VI) at acidic condition can be ascribed to the large attractive electrostatic forces between positive adsorbent surface charges and $Cr_2O_7^{-2}$ anion molecules. However, lower amount of Cr(VI) removal efficiency at high pH values would be derived from the competition between the chromate (CrO_4^{-2}) and OH^- ions for covering reactive surface sites. In addition, at higher pH values, the electrostatic repulsion between the negatively charged adsorbed ions and the negatively charged adsorbent surface reduces the Cr(VI) adsorption. However, pH of 3 was selected as an optimum value for Cr(VI) adsorption as reported in other studies [38]. The surfaces of adsorbent have occupied by some carboxylic groups (–COOH) and hydroxylic groups (–OH) after acid treatment. In acidic conditions, the positive surface charges can be formed, due to the protonation of electron π rich areas on the surface of adsorbent. Under these conditions, the application of negatively charged Cr(VI) ions is high. When pH decreases, the carboxylic groups are ionized and the negative charge density on the surface will be decreased.

3.3. Effect of contact time on Cr(VI) adsorption onto COOH@NPG/Fe_3O_4

The contact time is one of the most essential parameters in designing a batch that affects the adsorption of contaminants. Therefore, in this research, Cr(VI) adsorption was performed at contact time of 5–120 min while the other experimental parameters such as solution pH, adsorbent dosage, initial Cr(VI) concentration, agitation speed kept constant at 3, 35 mg/L, 100 mg/L and 200 rpm, respectively. As shown in Fig 3, considerable amounts of Cr(VI) were adsorbed onto COOH@NPG/Fe_3O_4 surfaces within the first 40 min and finally reached the equilibrium point after 60 min. Thus, 60 min was chosen as an equilibrium time in the optimal conditions and used in the future experiments. In other words, the availability of Cr(VI) adsorption to the active sites on the adsorbent surface did not show significant changes after 60 min.

3.4. Effect of adsorbent dosage on Cr(VI) adsorption onto COOH@NPG/Fe_3O_4

The effect of different absorbent concentrations (20, 35, 50, 100, 150 , 200, 250 and 300 mg/L) on the Cr(VI) removal from aqueous solution at pH solution of 3, 60 min of contact time, initial Cr(VI) concentration of 100 mg/L and agitation speed 200 rpm was performed in Fig 4. There are a few reports that the treated waste newspaper (TWNP) can be used for the removal of Cr(VI). The percentage of adsorbent increases by increase in the amount of adsorbent [39]. The reason of this process can be justified by increasing the accessibility of active vacant porous sites on the COOH@NPG/Fe_3O_4 surface for Cr(VI) adsorption.

3.5. Effect of different initial Cr(VI) concentrations on Cr(VI) adsorption onto COOH@NPG/Fe_3O_4

The effect of various initial Cr(VI) concentrations (25, 50, 100, 150 and 200 mg/L) on Cr(VI) adsorptive removal under optimum conditions (solution pH of 3, contact time of 60 min, agitation speed of 200 rpm and adsorbent dosage of 200 mg/L) is shown in Fig 5. This result shows that when the initial Cr(VI) concentration increased from 25 to 200 mg/L, Cr(VI) removal efficiency rate decreased gradually and reached the equilibrium state by decreasing the number of vacant nano-porous reactive surface sites. Similar trends were also observed where the adsorption percentage was increased with decreasing initial contaminant concentrations [38–40]. Synthesis of nano-adsorbent produces large external surface area and suitable pore size with sufficient volume provided well contact efficiency with Cr(VI) ions. The most possible proof for this process would be ascribed to the existence of abundant vacant nano-porous sites on COOH@NPG/Fe_3O_4 surface, which is filled with an enhancement in initial Cr(VI) ions concentrations. This results show that the functionalization of nano-porous

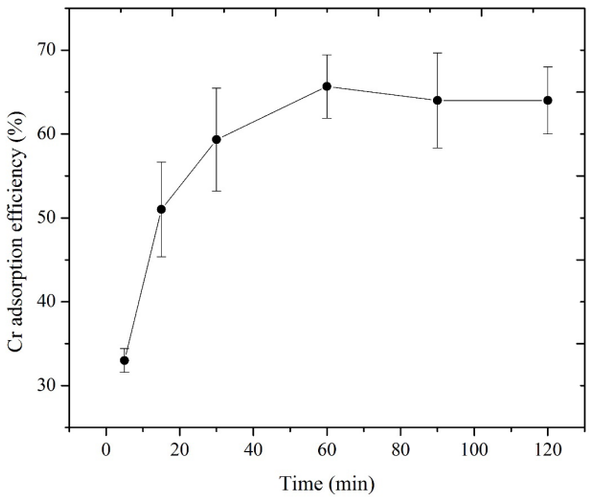

Fig. 3. Effect of contact time on the adsorption of Cr(VI) onto COOH@NPG/Fe_3O_4 (pH = 3, adsorbent dosage = 35 mg/L, initial Cr (VI) concentration = 100 mg/L and agitation speed = 200 rpm).

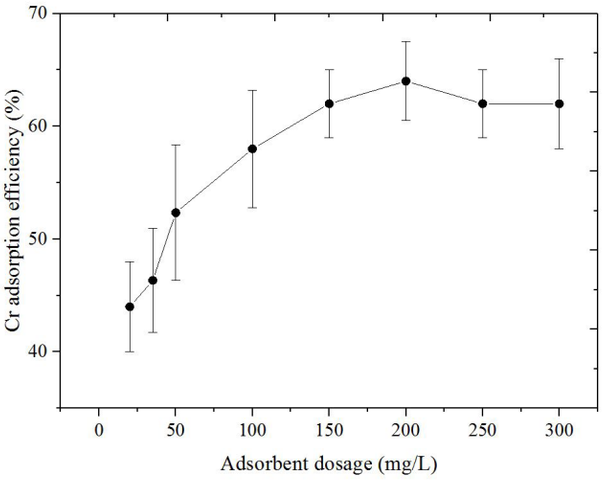

Fig. 4. Effect of adsorbent dose on the adsorption of Cr(VI) onto COOH@NPG/Fe_3O_4 (pH = 3, time = 60 min, initial Cr (VI) concentration = 100 mg/L and agitation speed = 200 rpm).

graphene not only has a positive impact on increasing the removal of chromium but may also have a negative impact on adsorbing porous building demolition during functionalization process [40].

3.6. Adsorption isotherm models

The equilibrium adsorption study via several most common models are applied in order to have better explanation of adsorptive interaction between adsorbent and adsorbate that is a very critical parameter in optimization of a batch system. Fig. 6 shows the Langmuir and Freundlich isotherm graphs of Cr(VI) on the adsorbent. Table 2 illustrates the obtained isotherm parameters from Langmuir and Freundlich models from adsorption of Cr(VI) onto the surfaces of

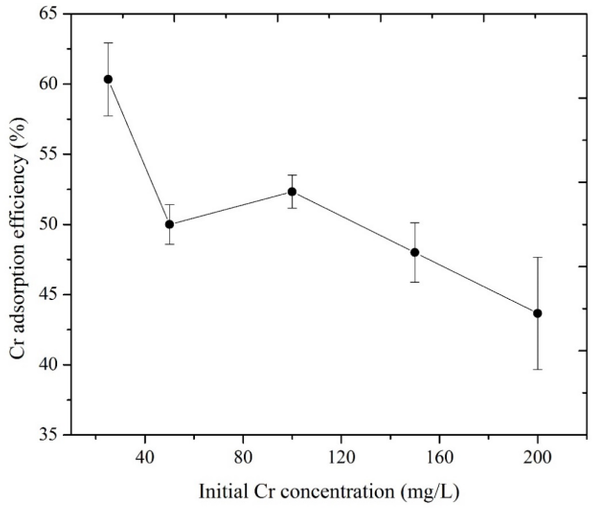

Fig. 5. Effect of initial Cr(VI) concentrations on the adsorption of (Cr(VI)) ions onto COOH@NPG/Fe_3O_4 (pH =3, time: 60 min, adsorbent dosage = 200 mg/L and agitation speed = 200 rpm).

COOH@NPG/Fe_3O_4 at ambient temperature and optimum conditions. The obtained coefficient of correlation (R^2) for COOH@NPG/Fe_3O_4 adsorbent illustrates that Langmuir model with significant R^2 (>0.99) had higher ability than Freundlich to fit the experimental data of Cr(VI) adsorptive removal at optimum experimental conditions (25 to 200 mg/L initial Cr(VI) concentrations, pH of solution 3, the contact time of 60 min, adsorbent dosage of 200 mg and agitation speed of 200 rpm).The Langmuir isotherm assumes monolayer sorption, which is derived from a certain quantity of reactive sites onto the surfaces of adsorbent. Based on the table, the maximum adsorption capacity (q_m) of Langmuir model is a relatively big value. It is also observed that the values of R_L lie between 0 and 1, indicating the favorable conditions for Cr(VI) adsorption. The rates of K_f and $1/n$ are calculated from the intercept and slope of the plot of log q_e vs. log C_e in Fig. 4 (a and b), respectively. Having a closer look to Table 2, when the amount of K_f value increased, the adsorption capacity of the adsorbent was increased as well. It can be inferred that Cr(VI) adsorption on the adsorbents at ambient temperature and optimal condition (solution pH of 3, contact time of 60 min, agitation speed of 200 rpm and adsorbent dosage of 200 mg/L) represents beneficial adsorption.

3.7. Kinetic study

Table 3 shows the adsorption kinetic parameters and related coefficient of correlation of Cr(VI) adsorptive removal onto the surfaces of COOH@NPG/Fe_3O_4. In addition, the kinetic plots of pseudo-first-order and pseudo-second-order models are illustrated in Fig 7. Based on the regression coefficient (R^2) in Table 3, the adsorption kinetic data was well-fitted by the pseudo-second-order model. In addition, the calculated equilibrium adsorption capacity, $q_{e,cal}$, using pseudo-second-order model was very close to the experimental $q_{e,exp}$ values, which confirms that the experimental data were better described by this model.

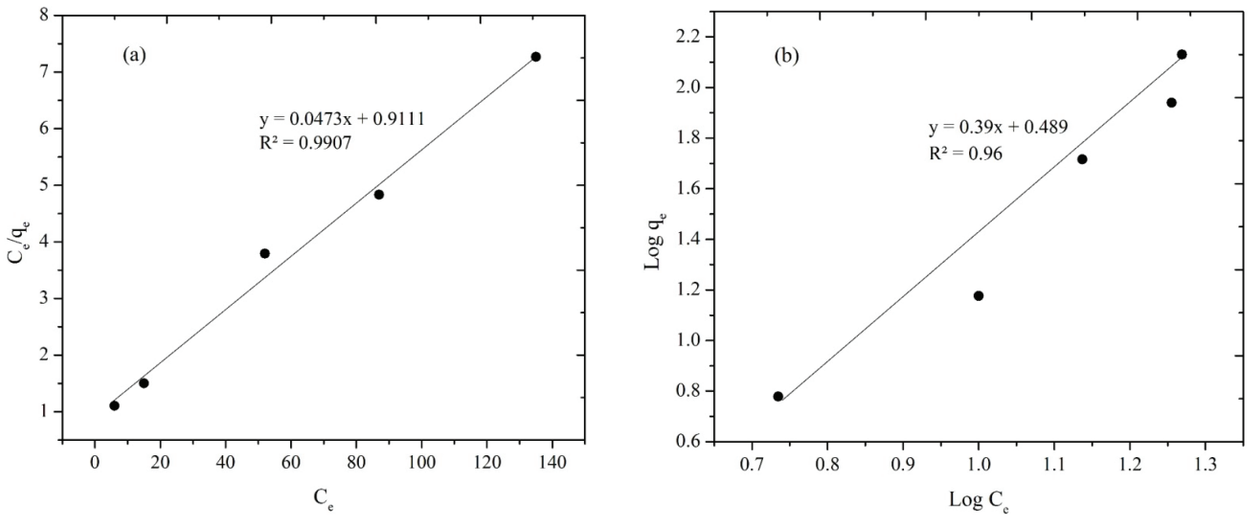

Fig. 6. The Langmuir (a), Freundlich (b) isotherm models for the adsorption of (Cr(VI)) ions on COOH@NPG/Fe_3O_4(pH = 3, time = 60 min, adsorbent dosage = 200 mg/L and agitation speed = 200 rpm).

Table 2
The parameters of the adsorption isotherm models in optimum conditions (pH = 3, contact time = 60 min, agitation speed 200 rpm, m_0 = 200 mg/L)

Isotherm models	Parameters	Value
Langmuir	q_m (mg/g)	21.14
	k_L(L/mg)	0.052
	R_L	0.087–0.43
	R^2	0.99
Freundlich	k_f (mg/g(L mg)/n)	3.02
	n	2.63
	R^2	0.96

Table 3
The parameters of the adsorption kinetic models (b) in optimum conditions (pH = 3, time = 60 min, adsorbent dosage = 200 mg/L and agitation speed= 200 rpm)

Kinetic models	Parameters	Value
Pseudo-first-order	$q_{e,cal}$(mg/g)	2.81
	k_1(min^{-1})	0.056
	R^2	0.94
Pseudo-second-order	$q_{e,cal}$(mg/g)	24.33
	k_2(g/mg)(min^{-1})	0.007
	R^2	0.99
	$q_{e,exp}$ (mg/g)	22.85

Similar results were also reported by the other researchers that showed pseudo-second-order model fitted better the experimental data [41]. This model suggests that the rate of adsorption process appeared to be controlled by chemical process involving valence forces through sharing or exchanging the electrons between the ions of Cr(VI) ions and the binding sites of adsorbent [42]. The quick increase of the adsorption rate in initial times could be due to the existence of large vacant active porous sites on the COOH@NPG/Fe_3O_4 surfaces. After passing the time, these volumes of porous sites are saturated by the Cr(VI). Active nano-porous sites on the adsorbent surfaces finally became limited and the process reached to the equilibrium state after this time period.

3.8. Thermodynamic of adsorption

Fig. 8 shows the thermodynamic diagram of Cr(VI) adsorption on NPG/Fe_3O_4@COOH. Results were also obtained by the curve where the values of $\Delta H°$ and $\Delta S°$ can be achieved from the slope and intercept of the plot of ln$K°$ against 1/T, respectively. The values of $\Delta H°$, $\Delta S°$, and $\Delta G°$ are represented in Table 4. The positive value of $\Delta H°$confirms the endothermic nature of the adsorption process and higher adsorption can be obtained at higher temperatures. The negative $\Delta G°$ values determine that the reaction rate decreases with an increase in the temperature and adsorption behavior of Cr(VI) on adsorbents are more spontaneous process at higher temperatures [43]. The positive values of $\Delta S°$ confirms an affinity between the Cr(VI) and adsorbents surface, and the degree of dispersion of the process increased with rising in temperature.

3.9. Comparison of maximum adsorption capacity of different adsorbents

A comparison between adsorption capacities of the synthesized adsorbent with various adsorbents for the removal of Cr(VI) reported in the literature are presented in Table 5. As it can be seen, the q_m value of NPG/Fe_3O_4@COOH for Cr(VI)are higher than that of the majority of

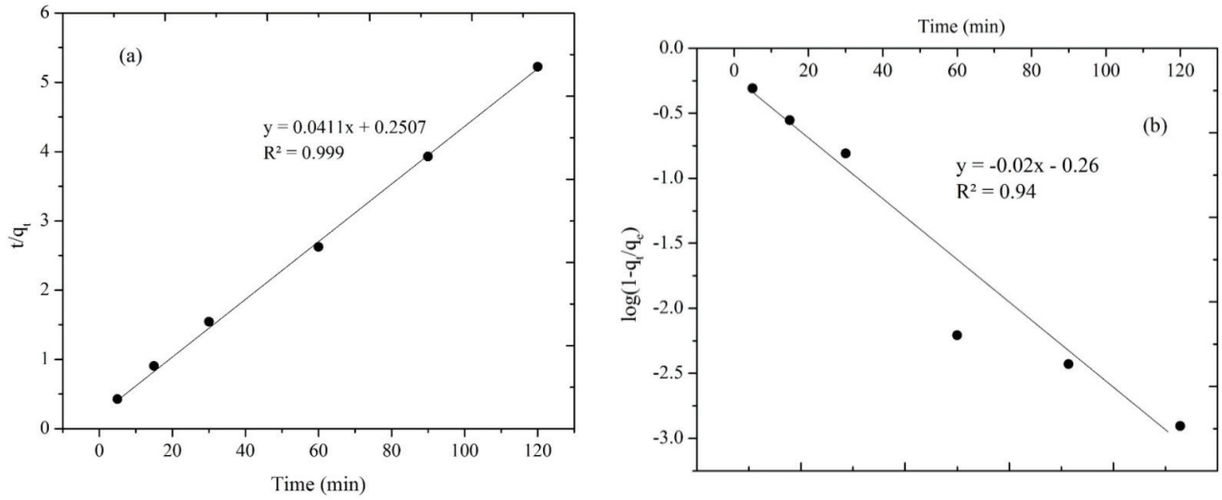

Fig. 7. Pseudo-first-order (a) and pseudo-second-order kinetic (b) models of (Cr(VI)) ions adsorption on COOH@NPG/Fe_3O_4 (pH = 3, time = 60 min, adsorbent dosage = 200 mg/L and agitation speed = 200 rpm).

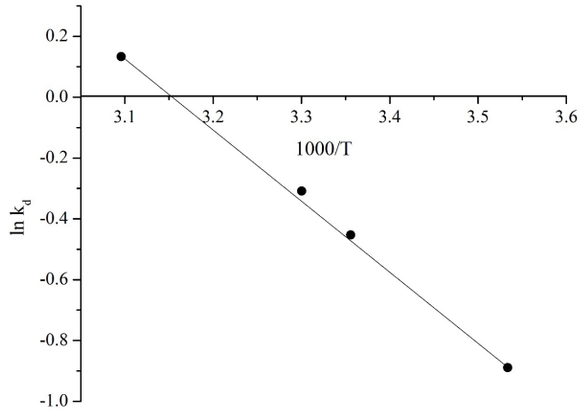

Fig. 8. The thermodynamic diagram of (Cr(VI)) ions adsorption onto COOH@NPG/Fe_3O_4 (pH = 3, time = 60 min, adsorbent dosage = 200 mg/L and agitation speed = 200 rpm).

Table 4
Thermodynamic parameters of Cr(VI) adsorption onto COOH@NPG/Fe_3O_4 (pH = 3, time = 60 min, adsorbent dosage = 200 mg/L and agitation speed = 200 rpm)

Temperature (K)	lnk_d	$\Delta G°$ (kJ/mol)	$\Delta H°$ (kJ/mol)	$\Delta S°$ (kJ/mol·K)
283	0.89	–2.09	19.43	0.06
298	0.45	–1.12		
303	0.31	–0.78		
323	0.13	–0.76		

other adsorbents previously reported in literature. These results demonstrate that the as-synthesized adsorbent has a good maximum adsorption capacity in comparison with the other applied adsorbents, and its can be considered as one of the most effective adsorbents for Cr(VI) adsorption. This study compared to previous research carried out magnetic nano-porous graphene adsorbent to the magnetic nano-porous graphene functionalized by carboxyl group decreased the removal efficiency and maximum adsorption capacity decreased from 43.5 to 23.5 mg/g. The obtained results revealed that the functionalization process of adsorbents has a negative impact onto their adsorption features thereby destruction of their porosity.

4. Conclusion

In this study, nano-porous graphene (NPG) was synthesized by chemical vapor deposition (CVD) method then magnetized by Fe_3O_4 and Fe_2O_3 powder for both rapid and economic separation by an external magnetic field, due to its magnetism contributed with Fe_3O_4. The NPG/Fe_3O_4 was also functionalized with carboxyl (COOH@NPG/Fe_3O_4) for using as an adsorbent for Cr(VI) removal from aqueous solution. The structural, functional and morphological properties of synthesized adsorbent were characterized using SEM, TEM, XRD, FTIR and VSM techniques. The optimum experimental conditions of Cr(VI) removal using NPG/Fe_3O_4 were investigated in batch adsorption experiments. The adsorption efficiency of Cr(VI) was increased with decreasing solution pH and initial Cr(VI) concentrations. But, an increasing trend was happened in Cr(VI) adsorption efficiency with increasing the adsorbent dosage and contact time until 60 min. In addition,the adsorption data was fitted well with Langmuir isotherm model. The Langmuir model indicated that it is monolayer adsorption of Cr(VI) on the COOH@NPG/Fe_3O_4 surface. Kinetic data of adsorption can be best described by a pseudo-second-order model. The sorption reaction onto adsorbent was an endothermic and spontaneous process in nature. It should be noted that the synthesized adsorbent has promising potential in wastewater treatment which can easily be separated via an external magnet.

Table 5
Comparison of maximum sorption capacities of various adsorbents for (Cr(VI)) ions removal

Adsorbent	pH	Isotherm	Kinetic	q_m (mg/g)	References
Raw activated carbon (AC)	3	Langmuir	pseudo-second-order	2.024	[37]
Modified activated carbon (AC)	3	Langmuir	pseudo-second order	1.805	
Raw carbon nano tube (CNT)	3	Langmuir	Pseudo-second-order	1.021	
Modified carbon nanotubes (CNTs)	3	Langmuir	pseudo-second-order	0.964	
Single/multi-walled carbon nanotubes	4	Langmuir	pseudo-second-order	20.30	[43]
Chitosan/zeolite film	4	Langmuir	pseudo-second-order	17.28	[44]
Arachis hypogeal shell in the form of beads (AHSB)	2	Langmuir	pseudo-second-order	6	[45]
functionalized carbon nanotubes by carboxylic groups	–	Langmuir	pseudo-second-order	47.62	[46]
CeO_2/ACNTs (Ceria nanoparticles supported on aligned carbon nanotubes)	7	Langmuir	pseudo-second-order	30.2	[47]
Sawdust	2	Langmuir	pseudo-second-order	58.82	[33]
NPG/Fe_3O_4	3	Langmuir	pseudo-second-order	43.5	[40]
COOH@NPG/Fe_3O_4	3	Langmuir	pseudo-second-order	21.14	This study

Acknowledgements

The authors are grateful for the support received from the Research Institute of Tehran Petroleum Industry. We express particular appreciation to Mr. Babak Kakavandi and Masoud Moradi for his academic assistance to improve the quality of our paper.

Conflict of interest

The authors declare that they have no conflict of interests.

References

[1] N. Sezgin, A. Yalçın, Y. Köseoğlu, $MnFe_2O_4$ nano spinels as potential sorbent for adsorption of chromium from industrial wastewater, Desal. Water Treat., 57 (2016) 16495–16506.
[2] A.V. Borhade, B.K. Uphade, Removal of chromium (VI) from aqueous solution using modified CdO nanoparticles, Desal. Water Treat., 57 (2016) 9776–9788.
[3] Y.-G. Zhao, H.-Y. Shen, S.-D. Pan, M.-Q. Hu, Q.-H. Xia, Preparation and characterization of amino-functionalized nano-Fe_3O_4 magnetic polymer adsorbents for removal of chromium (VI) ions, J. Mater. Sci., 45 (2010) 5291–5301.
[4] Z. Hu, X. Chen, Y. Zhao, T. Tian, G. Jin, Y. Shu, Y. Chen, L. Xu, K. Zen, C. Zhang, Serum MicroRNA signatures identified in a genome-wide serum MicroRNA expression profiling predict survival of non–small-cell lung cancer, J. Clin. Oncology., 28 (2010) 1721–1726.
[5] W. Mertz, The newer essential trace elements, chromium, tin, vanadium, nickel and silicon, Proc. Nutrit. Soc., 33 (1974) 307–313.
[6] T. Wang, J. Pan, X. Liu, Characterization of heavy metal contamination in the soil and sediment of the Three Gorges Reservoir, J. Environ. Sci. Health., Part A, (2016) 1–9.
[7] W. Roshan Singh, S. Kumar Pankaj, J. Singh, A.S. Kalamdhad, Reduction of bioavailability of heavy metals during vermicomposting of phumdi biomass of Loktak Lake (India) using Eisenia fetida, Chem. Speciation Bioavail., 26 (2014) 158–166.
[8] S. Chakraborty, J. Dasgupta, U. Farooq, J. Sikder, E. Drioli, S. Curcio, Experimental analysis, modeling and optimization of chromium (VI) removal from aqueous solutions by polymer-enhanced ultrafiltration, J. Membr. Sci., 456 (2014) 139–154.
[9] A.R. Esfahani, A.F. Firouzi, G. Sayyad, A. Kiasat, Isotherm study of cadmium adsorption onto stabilized-zerovalent iron nanoparticles, Int. J. Agronomy.Plant. Production., 4 (2013) 3444–3454.
[10] Y.-G. Zhao, H.-Y. Shen, S.-D. Pan, M.-Q. Hu, Synthesis, characterization and properties of ethylenediamine-functionalized Fe_3O_4 magnetic polymers for removal of Cr(VI) in wastewater, J. Hazard. Mater., 182 (2010) 295–302.
[11] L. Dong, W. Liu, R. Jiang, Z. Wang, Study on the adsorption mechanism of activated carbon removing low concentrations of heavy metals, Desal. Water Treat., 57 (2016) 7812–7822.
[12] O. Hamdaoui, Removal of copper(II) from aqueous phase by Purolite C100-MB cation exchange resin in fixed bed columns: Modeling, J. Hazard. Mater., 161 (2009) 737–746.
[13] G. Hota, B.R. Kumar, W. Ng, S. Ramakrishna, Fabrication and characterization of a boehmite nanoparticle impregnated electrospun fiber membrane for removal of metal ions, J. Mater. Sci., 43 (2008) 212–217.
[14] K. Sumathi, S. Mahimairaja, R. Naidu, Use of low-cost biological wastes and vermiculite for removal of chromium from tannery effluent, Bioresour. Technol., 96 (2005) 309–316.
[15] D. Gang, W. Hu, S.K. Banerji, T.E. Clevenger, Modified poly (4-vinylpyridine) coated silica gel. Fast kinetics of diffusion-controlled sorption of chromium (VI), Ind. Eng. Chem. Res., 40 (2001) 1200–1204.
[16] A.V. De Parga, F. Calleja, B. Borca, M. Passeggi Jr, J. Hinarejos, F. Guinea, R. Miranda, Periodically rippled graphene: growth and spatially resolved electronic structure, Phys. Rev. Lett., 100 (2008) 056807.
[17] Y. Pan, H. Zhang, D. Shi, J. Sun, S. Du, F. Liu, H.j. Gao, Highly ordered, millimeter-scale, continuous, single-crystalline graphene monolayer formed on Ru (0001), Adv. Mater., 21 (2009) 2777–2780.
[18] S. Li, X. Lu, Y. Xue, J. Lei, T. Zheng, C. Wang, Fabrication of polypyrrole/graphene oxide composite nanosheets and their applications for Cr(VI) removal in aqueous solution, PLoS One, 7 (2012) e43328.
[19] A. Mohseni-Bandpi, B. Kakavandi, R.R. Kalantary, A. Azari, A. Keramati, Development of a novel magnetite–chitosan composite for the removal of fluoride from drinking water: adsorption modeling and optimization, RSC Adv., 5 (2015) 73279–73289.

[20] B. Kakavandi, R.R. Kalantary, A.J. Jafari, S. Nasseri, A. Ameri, A. Esrafili, A. Azari, Pb (II) adsorption onto a magnetic composite of activated carbon and superparamagnetic Fe_3O_4 nanoparticles: Experimental and modeling study, CLEAN–Soil, Air, Water, (2015).
[21] B. Kakavandi, A. Esrafili, A. Mohseni-Bandpi, A.J. Jafari, R.R. Kalantary, Magnetic Fe_3O_4@ C nanoparticles as adsorbents for removal of amoxicillin from aqueous solution, Water Sci. Technol., 69 (2014).
[22] S. Nethaji, A. Sivasamy, A. Mandal, Preparation and characterization of corn cob activated carbon coated with nano-sized magnetite particles for the removal of Cr(VI), Bioresour. Technol., 134 (2013) 94–100.
[23] R. Muñoz, C. Gómez-Aleixandre, Review of CVD synthesis of graphene, Chem. Vap. Deposition., 19 (2013) 297–322.
[24] X. Li, W. Cai, J. An, S. Kim, J. Nah, D. Yang, R. Piner, A. Velamakanni, I. Jung, E. Tutuc, Large-area synthesis of high-quality and uniform graphene films on copper foils, Sci. Total Environ., 324 (2009) 1312–1314.
[25] S. Bae, H. Kim, Y. Lee, X. Xu, J.-S. Park, Y. Zheng, J. Balakrishnan, T. Lei, H.R. Kim, Y.I. Song, Roll-to-roll production of 30-inch graphene films for transparent electrodes, Nat. Nano. Tech., 5 (2010) 574–578.
[26] S. Pourmand, M. Abdouss, A. Rashidi, Fabrication of nanoporous graphene by chemical vapor deposition (CVD) and its application in oil spill removal as a recyclable nanosorbent, J. Ind. Eng. Chem., 22 (2015) 8–18.
[27] B. Li, H. Cao, J. Shao, G. Li, M. Qu, G. Yin, Co_3O_4@graphene composites as anode materials for high-performance lithium ion batteries, Inorg. Chem., 50 (2011) 1628–1632.
[28] H. Sadegh, K. Zare, B. Maazinejad, R. Shahryari-ghoshekandi, I. Tyagi, S. Agarwal, V.K. Gupta, Synthesis of MWCNT-COOH-Cysteamine composite and its application for dye removal, J. Mol. Liq., 215 (2016) 221–228.
[29] B. Kakavandi, A. Jonidi, R. Rezaei, S. Nasseri, A. Ameri, A. Esrafily, Synthesis and properties of Fe_3O_4-activated carbon magnetic nanoparticles for removal of aniline from aqueous solution: equilibrium, kinetic and thermodynamic studies, Iranian, J. Environ.Health. Sci. Eng., 10 (2013) 19.
[30] C. Hou, Q. Zhang, M. Zhu, Y. Li, H. Wang, One-step synthesis of magnetically-functionalized reduced graphite sheets and their use in hydrogels, Carbon, 49 (2011) 47–53.
[31] H. Sadegh, R. Shahryari-ghoshekandi, S. Agarwal, I. Tyagi, M. Asif, V.K. Gupta, Microwave-assisted removal of malachite green by carboxylate functionalized multi-walled carbon nanotubes: Kinetics and equilibrium study, J. Mol. Liq., 206 (2015) 151–158.
[32] O. Moradi, K. Zare, Adsorption of Pb (II), Cd (II) and Cu (II) ions in aqueous solution on SWCNTs and SWCNT–COOH surfaces: kinetics studies, Fullerenes, Nanostruct. Mater., 19 (2011) 628–652.
[33] V. Vinodhini, N. Das, Relevant approach to assess the performance of sawdust as adsorbent of chromium (VI) ions from aqueous solutions, Int. J. Environ. Sci. Technol., 7 (2010) 85–92.
[34] H. Gu, S.B. Rapole, Y. Huang, D. Cao, Z. Luo, S. Wei, Z. Guo, Synergistic interactions between multi-walled carbon nanotubes and toxic hexavalent chromium, J. Mat. Chem A., 1 (2013) 2011–2021.
[35] J. Zhu, S. Wei, H. Gu, S.B. Rapole, Q. Wang, Z. Luo, N. Haldolaarachchige, D.P. Young, Z. Guo, One-pot synthesis of magnetic graphene nanocomposites decorated with core@ double-shell nanoparticles for fast chromium removal, Environ. Sci. Technol., 46 (2011) 977–985.
[36] H. Gu, S.B. Rapole, J. Sharma, Y. Huang, D. Cao, H.A. Colorado, Z. Luo, N. Haldolaarachchige, D.P. Young, B. Walters, Magnetic polyaniline nanocomposites toward toxic hexavalent chromium removal, RSC Advances, 2 (2012) 11007–11018.
[37] C. Xu, B. Qiu, H. Gu, X. Yang, H. Wei, X. Huang, Y. Wang, D. Rutman, D. Cao, S. Bhana, Synergistic interactions between activated carbon fabrics and toxic hexavalent chromium, J. Solid State Technol., 3 (2014) M1–M9.
[38] Ihsanullah, F.A. Al-Khaldi, B. Abu-Sharkh, A.M. Abulkibash, M.I. Qureshi, T. Laoui, M.A. Atieh, Effect of acid modification on adsorption of hexavalent chromium (Cr(VI)) from aqueous solution by activated carbon and carbon nanotubes, Desal. Water Treat., 57 (2016) 7232–7244.
[39] P. Singh, D. Tiwary, I. Sinha, Starch-functionalized magnetite nanoparticles for hexavalent chromium removal from aqueous solutions, Desal. Water Treat., 57 (2016) 12608–12619.
[40] S. Fathi, R. Rezaei Kalantary, A. Rashidi, A. Karbassi, Hexavalent chromium adsorption from aqueous solutions using nanoporous graphene/Fe_3O_4 (NPG/Fe_3O_4: modeling and optimization), Desal. Water Treat., 57 (2016) 28284–28293.
[41] T. Anirudhan, J. Nima, P. Divya, Adsorption of chromium (VI) from aqueous solutions by glycidylmethacrylate-grafted-densified cellulose with quaternary ammonium groups, Appl. Surf. Sci., 279 (2013) 441–449.
[42] R. Rezaei Kalantry, A. Jonidi Jafari, A. Esrafili, B. Kakavandi, A. Gholizadeh, A. Azari, Optimization and evaluation of reactive dye adsorption on magnetic composite of activated carbon and iron oxide, Desal. Water Treat., 57 (2016) 6411–6422.
[43] G. Li, V. Shrotriya, J. Huang, Y. Yao, T. Moriarty, K. Emery, Y. Yang, High-efficiency solution processable polymer photovoltaic cells by self-organization of polymer blends, Nat. Mater., 4 (2005) 864–868.
[44] A.C. Batista, E.R. Villanueva, R.V.S. Amorim, M.T. Tavares, G.M. Campos-Takaki, Chromium (VI) ion adsorption features of chitosan film and its chitosan/zeolite conjugate 13X film, Molecules, 16 (2011) 3569–3579.
[45] G. Mahajan, D. Sud, Kinetics and equilibrium studies of Cr(VI) metalion remediation by Arachis hypogea shells: A green approach, BioResources, 6 (2011) 3324–3338.
[46] R. Ghasemi, T. Sayahi, S. Tourani, M. Kavianimehr, Modified Magnetite Nanoparticles for Hexavalent Chromium Removal from Water, J. Dispersion Sci. Technol., 37 (2016) 1303–1314.
[47] Z.-C. Di, J. Ding, X.-J. Peng, Y.-H. Li, Z.-K. Luan, J. Liang, Chromium adsorption by aligned carbon nanotubes supported ceria nanoparticles, Chemosphere, 62 (2006) 861–865.